JACS
JOURNAL OF THE AMERICAN CHEMICAL SOCIETY

Article

pubs.acs.org/JACS

Multifunctional Fullerene Derivative for Interface Engineering in Perovskite Solar Cells

Yaowen Li,*[,†,‡] Yue Zhao,[†] Qi Chen,[‡] Yang (Michael) Yang,[‡] Yongsheng Liu,[‡] Ziruo Hong,*[,‡] Zonghao Liu,[‡] Yao-Tsung Hsieh,[‡] Lei Meng,[‡] Yongfang Li,*[,†] and Yang Yang*[,‡]

[†]Laboratory of Advanced Optoelectronic Materials, College of Chemistry, Chemical Engineering and Materials Science, Soochow University, Suzhou 215123, China

[‡]Department of Materials Science and Engineering, University of California, Los Angeles, California 90095, United States

Supporting Information

ABSTRACT: In perovskite based planar heterojunction solar cells, the interface between the TiO_2 compact layer and the perovskite film is critical for high photovoltaic performance. The deep trap states on the TiO_2 surface induce several challenging issues, such as charge recombination loss and poor stability etc. To solve the problems, we synthesized a triblock fullerene derivative (PCBB-2CN-2C8) via rational molecular design for interface engineering in the perovskite solar cells. Modifying the TiO_2 surface with the compound significantly improves charge extraction from the perovskite layer. Together with its uplifted surface work function, open circuit voltage and fill factor are dramatically increased from 0.99 to 1.06 V, and from 72.2% to 79.1%, respectively, resulting in 20.7% improvement in power conversion efficiency for the best performing devices. Scrutinizing the electrical properties of this modified interfacial layer strongly suggests that PCBB-2CN-2C8 passivates the TiO_2 surface and thus reduces charge recombination loss caused by the deep trap states of TiO_2. The passivation effect is further proven by stability testing of the perovskite solar cells with shelf lifetime under ambient conditions improved by a factor of more than 4, from ~40 h to ~200 h, using PCBB-2CN-2C8 as the TiO_2 modification layer. This work offers not only a promising material for cathode interface engineering, but also provides a viable approach to address the challenges of deep trap states on TiO_2 surface in planar perovskite solar cells.

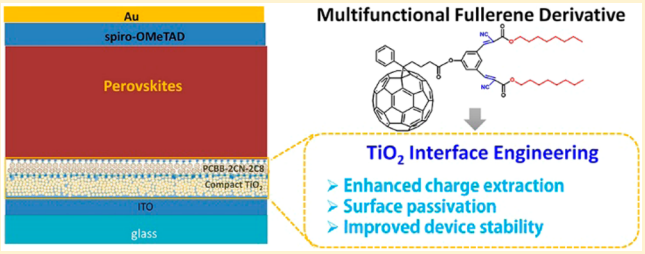

INTRODUCTION

Organic−inorganic metal halide perovskite solar cells have attracted growing interest recently, as its power conversion efficiency (PCE) rose to 20% within several years.[1−7] Although the perovskite solar cells based on meso-porous TiO_2 take the lead in the efficiency competition, planar structured perovskite solar cells are currently becoming popular due to their low temperature processing and simple device architecture. Nevertheless, the interface contacts in the devices are critically important for achieving high performance planar perovskite solar cells.[8−11]

The planar perovskite solar cells based on perovskite film as the photoactive layer can be classified as an n-i-p device structure[4,7] with indium−tin-oxide (ITO) or fluorine-doped tin-oxide (FTO) transparent electrode as the cathode or p-i-n device structure with ITO or FTO as the anode.[12−14] In the n-i-p structured perovskite solar cells, doped small molecules and polymers (such as spiro-OMeTAD), as well as polyelectrolytes, can be used as hole transport layers (p-type anode buffer layer, HTL), and some metal oxides (such as TiO_2), fullerenes, and their derivatives can be used as electron transport layers (n-type cathode buffer layer, ETL) on ITO or FTO electrode.[8] Only in some exceptional cases, either p- or n- type layers can be skipped for simplicity, while the penalty is the inevitable loss in charge recombination and build-in potential.[13−15] To effectively extract charge carriers, it is important for the charge transport layers to have high selectivity. For example, TiO_2 has been regarded as one of the best electron extraction and transport materials, due to its proper conduction band compatible with those of hybrid perovskites. In the meantime, the deep valence band is able to block the holes. Recent study also indicates that the low temperature processed TiO_2 layer is able to play such a critical role, which makes it an important electron transport layer for planar n-i-p perovskite solar cells.[15]

However, there are two drawbacks of low temperature processed TiO_2 as the electron transport layer in the planar perovskite solar cells. First, the low electron mobility results in charge accumulation in the TiO_2 layer. That means TiO_2 is not an ideal electron acceptor and transport layer for perovskite.[16,17] Second, exposure of TiO_2 to UV light further induces formation of oxygen vacancies, which are energetically deep trap levels responsible for severe recombination loss.[18,19] As a result, the TiO_2/perovskite interface slows down the photoresponse of the photovoltaic devices, causing strong hysteresis behaviors, and thus making accurate efficiency measurement

Received: October 10, 2015
Published: November 23, 2015

DOI: 10.1021/jacs.5b10614
J. Am. Chem. Soc. 2015, 137, 15540−15547

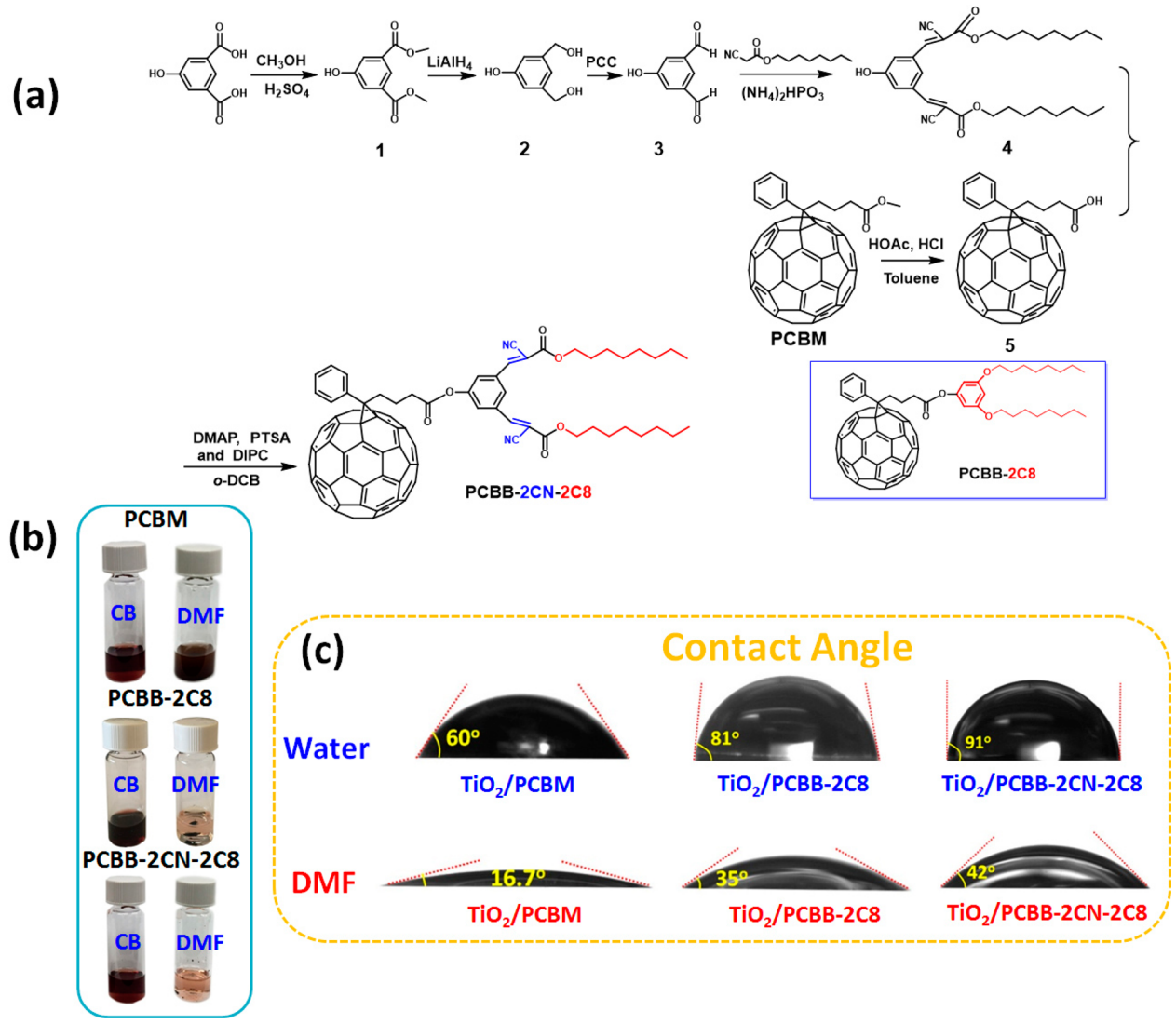

Figure 1. (a) Synthetic route and chemical structure of PCBB-2CN-2C8, and molecular structures of PCBM and PCBB-2C8 for comparison. (b) The photographs of PCBM, PCBB-2C8, and PCBB-2CN-2C8 in CB or DMF solution with concentration of 5 mg/mL. (c) The images of the water and DMF droplet contact angles on different surfaces of fullerene derivative-coated TiO_2.

difficult.[17] Snaith et al. proposed to replace TiO_2 with other inert metal oxides (Al_2O_3 etc.) through which highly stable perovskite solar cells have been demonstrated.[18] However, it remains challenging to identify a replacement that works as well as TiO_2, especially in planar heterojunction cells. As an alternative approach, coating n-type materials like [6,6]-Phenyl-C_{61}-butyric acid methyl ester (PCBM) offers competitive photovoltaic performance; however, since PCBM is soluble in *N*,*N*-dimethylformamide (DMF), it requires deposition of PbI_2 via thermal evaporation in high vacuum, which complexes the processing.[20] Another effective way to circumvent this challenge has been proposed to modify the TiO_2 surface using a self-assembled monolayer (SAM) of fullerene derivatives.[9,21] Yet the deposition of a SAM layer usually takes more than 10 h for the molecular anchoring, which is not convenient for both lab research and scale-up manufacturing. Taking these issues into consideration, it is urgent to explore alternatives to engineer the TiO_2 film surface, in order to achieve: (1) efficient electron collection and hole blocking; (2) simple and fast processing; and (3) high device stability against UV illumination. To satisfy the demand for surface modification on TiO_2 in perovskite solar cells, the interfacial materials should meet these criteria.

In this work, we tried to deal with multiple issues regarding using a triblock fullerene derivative [6,6]-phenyl-C_{61}-butyric acid-dioctyl-3,3′-(5-hydroxy-1,3-phenylene)-bis(2-cyanoacrylate) ester (PCBB-2CN-2C8) (as shown in Figure 1a) as a cathode modification layer on TiO_2. To have desirable electrical properties, we chose fullerene C_{60} as the main building block of the molecule because of its high electron affinity for efficient electron transfer. Electron-deficient cyano-groups were implanted for pacifying the oxygen vacancy. Since multilayer coating via solution process in the device fabrication of perovskite solar cells requires orthogonal solvents, we introduce dioctyloxy chains and cyano-groups to minimize its solubility in polar solvent, (such as DMF used for coating perovskite precursors) and to be highly soluble in nonpolar solvents like chlorobenzene (CB) for its solution-processing. The selective solubility enables us to fabricate all the functional layers via the solution process except for the metal electrodes. We then incorporated the PCBB-2CN-2C8 into n-i-p planar perovskite solar cells to modify the TiO_2 surface and obtained significantly

DOI: 10.1021/jacs.5b10614
J. Am. Chem. Soc. 2015, 137, 15540−15547

enhanced photovoltaic performance, as well as reduction of the hysteresis. Moreover, the shelf stability of unencapsulated devices under normal ambient conditions was significantly improved compared with the TiO_2 based control devices.

RESULTS AND DISCUSSION

The synthetic route of PCBB-2CN-2C8 is shown in Figure 1a. Reaction of fullerene acid (PCBA, compound 5) with dioctyl 3,3′-(5-hydroxy-1,3-phenylene)-bis(2-cyanoacrylate) (compound 4) in ortho-dichlorobenzene (*o*-DCB) using 4-dimethylamino-pyridine (DMAP), *p*-toluenesulfonamide (PTSA), and diisopropylcarbinol (DIPC) as catalysts gave the target PCBB-2CN-2C8, in 67% yield. In addition, PCBB-2CN-2C8 shows high thermal stability with both high decomposition temperature of ca. 356 °C (5% weight loss from thermal gravimetric analysis (TGA, in Supporting Information, SI, Figure S1) and amorphous nature (T_g detected at 49.7 °C, excluding obvious endothermic peaks, shown in Figure S2), which are beneficial for enduring high temperature and retaining a stable PCBB-2CN-2C8 film morphology at elevated temperature, respectively.[22] Besides, we measured the electron mobility (μ_e) of PCBB-2CN-2C8 using space-charge limited current measurement, as shown in Figure S3. It has a μ_e of 4.8×10^{-3} cm^2 $V^{-1}s^{-1}$, comparable to that of PCBM (2.5×10^{-3} cm^2 $V^{-1}s^{-1}$). Thus, PCBB-2CN-2C8 is good for electron transport.[15,23] Detailed synthetic procedure and characterization are described in the Experimental Section and the SI (Figures S4–S6). The molecular structures of PCBM and [6,6]-phenyl-C61-butyric acid-3,5-bis(octyloxy)-benzyl ester (PCBB-2C8) without cyano-groups are also shown in Figure 1a for comparison. Figure 1b shows the excellent solubility of PCBB-2CN-2C8 in CB (more than 100 mg/mL), while it is almost insoluble in DMF due to presence of dioctyloxy chains, consistent with our design consideration. This is important from a processing point of view, since DMF is a common solvent to synthesize lead iodide perovskite films. In comparison, PCBB-2C8 is more soluble in DMF than PCBB-2CN-2C8 due to the absence of cyano-groups. PCBM without long dioctyloxy chains and cyano-groups is well dissolved in both DMF and CB. Therefore, the films of PCBB-2C8 and PCBM cannot stand DMF solution coating.

Surface wetting is an important factor for the solution coating process. Generally, polar solvents have excellent wetting properties on TiO_2 surface, as confirmed by the extremely small contact angles of water and DMF (Figure S7). We tested if PCBB-2CN-2C8 in DMF solution was suitable for coating on TiO_2 surface by using contact angle measurement, and PCBM and PCBB-2C8 were used for comparison. In Figure 1c, water droplets on TiO_2/PCBM, TiO_2/PCBB-2C8, and TiO_2/PCBB-2CN-2C8 have contact angles of 60°, 81°, and 91°, respectively. Both PCBB-2C8 and PCBB-2CN-2C8 show larger contact angles than PCBM, indicating the octyloxy chains could be responsible for poor wetting. The cyano-groups in PCBB-2CN-2C8 make it more hydrophobic than PCBB-2C8. A similar trend holds for DMF, with slightly better wetting than water, and the strong hydrophilic property of PCBB-2CN-2C8 indicates its potential advantage for PbI_2 deposition from DMF solution.[24]

In attempt to integrate PCBB-2CN-2C8 in photovoltaic cells, we investigated the effect of PCBB-2CN-2C8 coated compact TiO_2 on the growth of a $CH_3NH_3PbI_3$ film via a two-step method. As shown in Figure S8, the pristine TiO_2 surface has a root-mean-square (rms) surface roughness of 4.43 nm. Coating PCBB-2CN-2C8 on TiO_2 slightly reduces the roughness to rms of 3.98 nm, which should not influence the growth of the perovskite crystal. Figure 2, parts a and b, shows top view

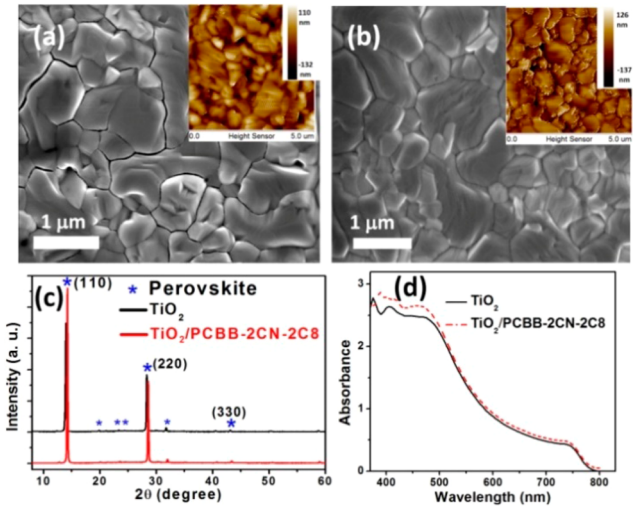

Figure 2. Top-view SEM images of perovskite films grown on (a) TiO_2 and (b) TiO_2/PCBB-2CN-2C8. The insets are respective AFM images. (c) XRD patterns of the perovskite films grown on TiO_2 and TiO_2/PCBB-2CN-2C8. (d) Absorption spectra of perovskite films grown on TiO_2 and TiO_2/PCBB-2CN-2C8.

images taken by scanning electron microscopy (SEM) and atomic force microscopy (AFM). We can see the compact film and homogeneous grain size distribution with an average value of 1097 nm (Figure S9). Without PCBB-2CN-2C8, perovskite crystals grown directly on the TiO_2 surface show a slight smaller grain size of 1035 nm with tiny cracks throughout the film. Both films have a similar surface roughness of about 27.0 nm. The observation suggests that a high-quality perovskite film with large grain size can be formed on the surface of TiO_2/PCBB-2CN-2C8, which is consistent with previous reports.[24,25]

The bulk properties of perovskite films strongly depend on their crystal quality. X-ray diffraction (XRD) was conducted to characterize the perovskite films grown on TiO_2 with and without PCBB-2CN-2C8. In Figure 2c, both samples show similar crystal structures with distinctive (110), (220), and (330) diffraction peaks at 14.2°, 28.4°, and 43.2°, respectively, in accordance with the major phases of $CH_3NH_3PbI_3$.[26] Similar to the film grown on the TiO_2 surface, we cannot see peaks from the impurity phase or significant change of the diffraction peak ratio, indicating a pure perovskite phase on both surfaces without any change in crystal orientation. The XRD peak at 14.2° becomes much stronger and sharper, as the full width at half-maximum (fwhm) of the peak (110) decreases from 0.188° on TiO_2 to 0.149° on TiO_2/PCBB-2CN-2C8. It agrees well with the improved perovskite film quality discussed in the previous section.

Figure 2d shows the ultraviolet–visible (UV–vis) absorption spectra of the perovskite films deposited on glass/ITO/TiO_2 and glass/ITO/TiO_2/PCBB-2CN-2C8 substrates. The sample with PCBB-2CN-2C8 shows a slightly enhanced absorption in the blue region due to the absorption of fullerene. Similarly, except for a slight drop in UV and blue range, the transmittance spectrum of the glass/ITO/TiO_2 substrates with PCBB-2CN-2C8 assembles that of the glass/ITO/TiO_2 control sample in the visible region (Figure S10)

DOI: 10.1021/jacs.5b10614
J. Am. Chem. Soc. 2015, 137, 15540–15547

We then fabricated the planar heterojunction perovskite photovoltaic cell with a structure of glass/ITO/TiO_2 (50 nm)/PCBB-2CN-2C8 (10 nm)/$CH_3NH_3PbI_3$ (290 nm)/spiro-OMeTAD (170 nm)/Au (120 nm) as illustrated in Figure 3a. Figure 3b provides the energy-level diagram. We can see

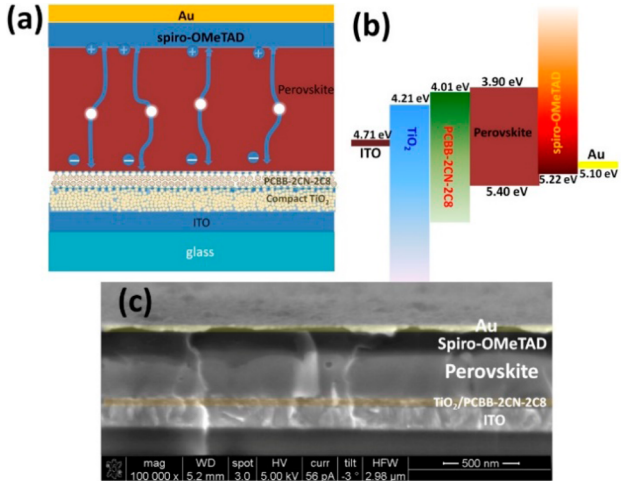

Figure 3. (a) perovskite solar cells architecture employing TiO_2/PCBB-2CN-2C8 as the ETL. (b) The corresponding energy-level diagram. (c) Cross-section SEM images of complete perovskite solar cell.

that the PCBB-2CN-2C8 layer between TiO_2 and perovskite does not change the overall energetic landscape, still allowing a cascade electron transfer process. Work function of TiO_2 is 4.21 eV measured by Kelvin probe force microscope (KPFM) (Figure S8), while that of PCBB-2CN-2C8 modified TiO_2 is uplifted by ~200 meV, reaching 4.01 eV.[27,28] As the conduction band bottom (ECB) of perovskite is 3.90 eV, the energy offset is sufficient for electron extraction from perovskite to the electron transport layer. In the cross-section SEM image in Figure 3c, all functional layers can be clearly distinguished. The grain sizes are obviously larger than the film thickness, giving an average grain size/film thickness aspect ratio of 3.8. The length of the grains is equal to the thickness of the film, and the film uniformity easily expands to several micrometers, as displayed. Meanwhile, combining the larger, compact and homogeneous grains in perovskite film on TiO_2/PCBB-2CN-2C8, the most of the grain boundaries perpendicular to the substrate can effectively minimize the grain boundary energy.[24]

J–*V* characteristics of the perovskite solar cells with or without PCBB-2CN-2C8 modification layer were measured under simulated solar illumination of AM1.5G 100 mW/cm^2. As shown in Figure 4a, while the TiO_2 ETL based device gave rise to a PCE of 13.35 ± 0.85% (the best PCE of 14.38%) from reverse scan,[20,21,29] we achieved a 16.45 ± 0.81% PCE (the best PCE of 17.35%) from the TiO_2/PCBB-2CN-2C8 based device. The key photovoltaic parameters are summarized in Table 1. The device employing PCBB-2CN-2C8 as TiO_2 modification layer yields improved V_{oc} from 0.98 ± 0.015 V to 1.06 ± 0.012 V, and FF from 70.2 ± 1.9% to 78.0 ± 1.0%. Theoretically, V_{oc} is determined by the quasi-Fermi level splitting in photoactive layer, and limited by the work function difference of two electrode contacts, i.e., TiO_2/PCBB-2CN-2C8 and spiro-MeOTAD.[3] The higher V_{oc} could be attributed to the lower work function of TiO_2/PCBB-2CN-2C8 (4.01 eV) than that of TiO_2 (4.21 eV). As discussed above, the well-defined perovskite

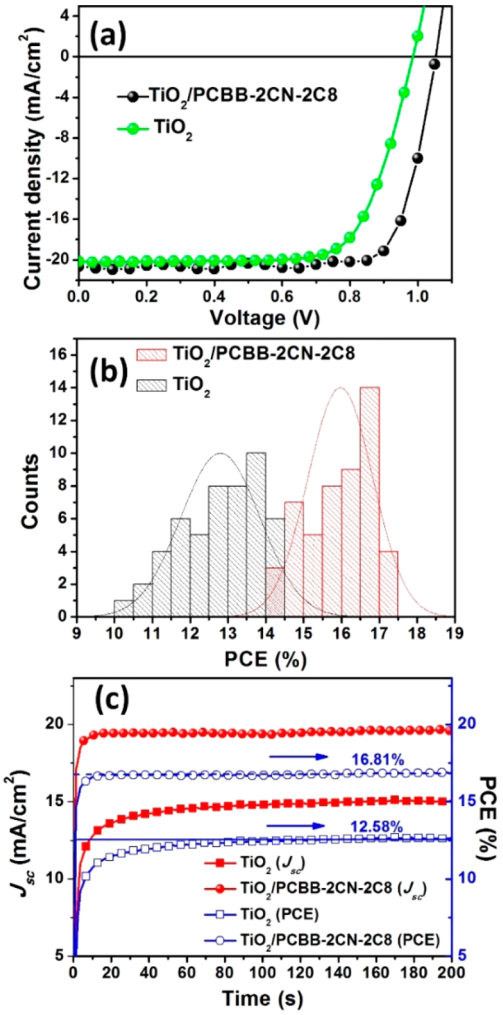

Figure 4. (a) *J*–*V* curves of perovskite solar cells with structure of glass/ITO/TiO_2/with or without PCBB-2CN-2C8/$MAPbI_3$/spiro-OMeTAD/Au under illumination of AM1.5G 100 mW/cm^2 simulated solar light. (b) Maximal steady-state photocurrent output at the maximum power point (for TiO_2 based device at 0.84 V, and TiO_2/PCBB-2CN-2C8 based device at 0.86 V) and their corresponding power output. (c) Histograms of device PCE measured for 50 devices based on TiO_2 and TiO_2/PCBB-2CN-2C8 ETLs.

film with high crystallinity, homogeneous crystal size distribution, and equal film thickness with grain size also can effectively depress bulk recombination and reduce shunting pathways.[30] It will, at least partially, account for the improved FF of 79.1% of the best device, which is high for perovskite photovoltaic devices.[15,31–33] External quantum efficiency (EQE) spectra of the perovskite solar cell are shown in Figure S11. Since the reproducibility of device efficiency has been a concern, we further show a histogram of the PCE of 50 perovskite solar cells based on TiO_2 and TiO_2/PCBB-2CN-2C8 ETLs in Figure 4c. It shows the top 1/3 of TiO_2/PCBB-2CN-2C8 ETL based devices delivered PCE over 16.5%, compared with 13.5% TiO_2 ETL-based devices. The improved device performance and encouraging reproducibility unambiguously revealed tremendous potential of molecular engineering of the cathode interface materials in perovskite solar cells. To avoid overestimation of photovoltaic efficiency caused by hysteresis, we took maximal steady-state power and photocurrent output in Figure 4c. TiO_2/PCBB-2CN-2C8 based cells

DOI: 10.1021/jacs.5b10614
J. Am. Chem. Soc. 2015, 137, 15540–15547

Table 1. Summary of Photovoltaic Parameters[a] of Perovskite Solar Cells with and without PCBB-2CN-2C8 Modification Layer

ETL	V_{oc} (V)	FF (%)	J_{sc} (mA/cm^2)	PCE (%)	
				average (best)	max. power output[b]
TiO_2 (RS)	0.98 ± 0.015 (0.99)	70.2 ± 1.9 (72.2)	19.23 ± 0.83 (20.18)	13.35 ± 0.85 (14.38)	12.58
TiO_2 (FS)	0.95 ± 0.010 (0.95)	61.0 ± 2.0 (62.1)	19.10 ± 0.76 (20.24)	10.95 ± 0.80 (11.95)	
TiO_2/PCBB-2CN-2C8 (RS)	1.06 ± 0.012 (1.06)	78.0 ± 1.0 (79.1)	19.85 ± 0.75 (20.68)	16.45 ± 0.81 (17.35)	16.81
TiO_2/PCBB-2CN-2C8 (FS)	1.05 ± 0.08 (1.04)	73.5 ± 1.2 (74.4)	19.7 ± 0.70 (20.54)	15.25 ± 0.60 (15.90)	

[a]Average and standard deviation values were obtained based on over 20 cells from 3 different batches for each ETL. FS: forward scan, scan rate 200 mV/s, delay time 100 ms; RS: reverse scan, scan rate 200 mV/s, delay time 100 ms. Parameters of the best cell are reported in brackets. [b]Maximal steady-state power output, which is equal the PCE of maximum power output.

delivered 19.55 mA/cm^2 at 0.86 V, corresponding to PCE of 16.81%, very close to the value from reverse bias scan (defined as from positive bias to negative). From the TiO_2 based control device, a PCE of 12.58% was determined. This experiment gives solid evidence for efficiency enhancement due to the TiO_2 ETL interfacial modification.

To further investigate the hysteresis issue, we then took scans in both the reverse and forward directions to compare the photoresponse behavior of the perovskite solar cells (see the details in Figure S12). Under forward and reverse scan, the TiO_2 based control device gives PCE of 11.95% and 14.38%, respectively, and the hysteresis index of 0.184 as calculated according to eq (1) in Supporting Information.[34] The perovskite solar cells with TiO_2/PCBB-2CN-2C8 ETL show a hysteresis index of 0.052, much less hysteresis than that of the control device. Consistently, as shown in Figure 4c, the device with the PCBB-2CN-2C8 modification layer shows a faster rising photocurrent to maximum value during immediate light illumination than that of the control device. Since the electrons have to flow through the TiO_2 layer, whether modified or not, the fast photoresponse should not be related to electron transport properties. However, considering the large amount of defects and interband states on the TiO_2 surface, the prompt photocurrent saturation could be related to the filling of these states. Therefore, we believe the passivation of the trap states by PCBB-2CN-2C8 is the key to reduce the hysteresis, as discussed later.[35]

In order to further look into the effect of PCBB-2CN-2C8 modification on the improvement of photovoltaic performance and reduction of hysteresis behavior, we investigated charge dynamics by measuring photoluminescence (PL) and time-resolved PL (TRPL) of the perovskite film on TiO_2 and TiO_2/PCBB-2CN-2C8. Figure 5a shows the steady-state PL spectra of perovskite films on TiO_2 and TiO_2/PCBB-2CN-2C8, respectively. The PL intensity of TiO_2/PCBB-2CN-2C8/perovskite was reduced by a magnitude of three-fold compared with that of TiO_2/Perovskite, while the absorbance of the two films are essentially the same. This result shows fast electron injection from perovskite into PCBB-2CN-2C8. It is well-known that fullerenes and their derivatives are strong electron acceptors, and the C_{60} carbon ball is able to accommodate even multiple electrons at the same time.[9] Thus, in spite of the lower energy offset for the electron transfer at the TiO_2/PCBB-2CN-2C8/perovskite interface, as shown in Figure 3b, the significant PL quenching confirms the good electronic coupling between the conduction band of perovskite and the LUMO of PCBB-2CN-2C8. Furthermore, the TRPL was measured by monitoring the peak emission at 768 nm, as shown in Figure 5b. Fitting the data with biexponential decay yields two time constants, i.e., τ_1 and τ_2, as summarized in Table S1). τ_1 represents the bulk recombination in perovskite bulk films in a

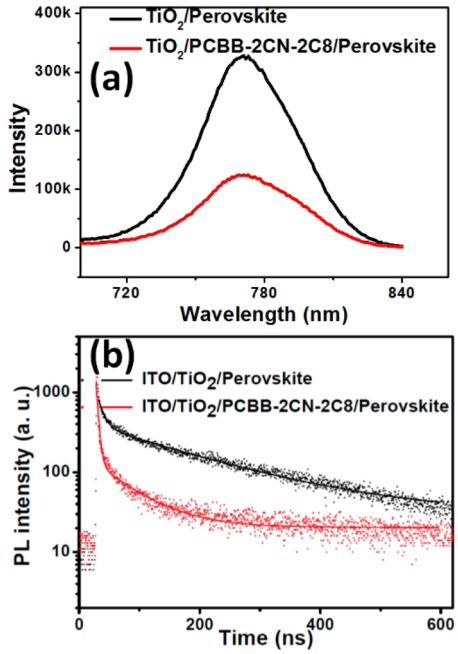

Figure 5. (a) The steady-state PL spectra of perovskite film on TiO_2 and TiO_2/PCBB-2CN-2C8. (b) TRPL decay transient spectra of ITO/TiO_2/perovskite and ITO/TiO_2/PCBB-2CN-2C8/perovskite.

relatively short time scale of a few tens of nanosecond, and the slow one, τ_2 ranging in hundred nanosecond, comes from the delayed recombination of trapped charges.[36,37] For TiO_2/perovskite, τ_1 is 9.7 ns with a 96.82% ratio and the τ_2 was 172.0 ns with a 3.18% ratio, suggesting that the depopulation of photogenerated charges was dominated by charge collection through the TiO_2/Perovskite interface, accompanied with weak delayed radiative recombination. As for TiO_2/PCBB-2CN-2C8/Perovskite, both τ_1 and τ_2 were shortened to 3.6 and 63.2 ns, respectively, and interestingly, τ_2 is almost overwhelmed by τ_1. It is not only because the modified TiO_2 induces fast electron transfer from perovskite film, but also very likely PCBB-2CN-2C8 reduces the trap state density of TiO_2 via passivation. This is consistent with enhanced J_{sc} and FF from a modified TiO_2-based device. As one can expect, the surface passivation on TiO_2 shall also be responsible for the lower hysteresis behavior, since the trap sites enable long existing charge carriers and thus slow down the device response speed.

To further understand the charge extraction and recombination processes, we characterized transient photocurrent decay (see the experimental details in the SI) as shown in Figure 6a. The TiO_2/PCBB-2CN-2C8 ETL-based device shows a faster decay compared with that of the TiO_2-based control device, which confirms the strong electron accepting properties of

DOI: 10.1021/jacs.5b10614
J. Am. Chem. Soc. 2015, 137, 15540−15547

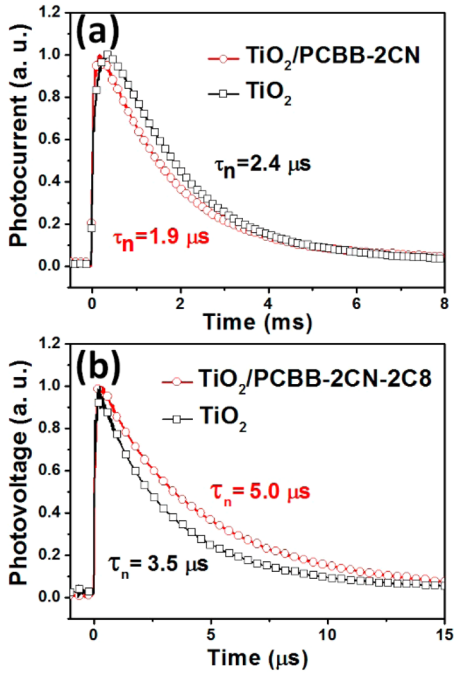

Figure 6. (a) Transient photocurrent decay and (b) transient photovoltage decay of the optimized devices employing the $TiO_2$and TiO_2/PCBB-2CN-2C8 as ETLs.

PCBB-2CN-2C8. We further investigate how PCBB-2CN-2C8 affects carrier recombination dynamics in the photovoltaic device. Transient photovoltage (TPV) decay was performed under open circuit conditions under a white light bias equal to 0.5 sun intensity (see the experimental details in the SI). The photovoltage signal is triggered by a pulse light that pumps up the carrier density and thus quarsi-Fermi level splitting, and the charge carriers through recombination are directly measured via monitoring the photovoltage decay.[38,39] The photovoltage decay curves of the perovskite solar cells based on TiO_2 and TiO_2/PCBB-2CN-2C8 ETLs are plotted in Figure 6b. In both cases, the photovoltage decay constants are on the scale of microseconds, in accordance with a recent report.[6] The fast component of the TPV decay is typically associated with nongerminate recombination.[38,39] The carrier lifetime in the PCBB-2CN-2C8-based device was measured to be ~1.5 times longer than that of the TiO_2-based device, consistent with the higher V_{oc}, J_{sc}, and FF we observed due to insertion of PCBB-2CN-2C8. Again our observation supported the argument that the passivation of the trap states on the TiO_2 surface can efficiently suppress the charge recombination.

In view of the similar film quality of perovskite on both TiO_2 and TiO_2/PCBB-2CN-2C8 surfaces, we speculate that the increase in carrier lifetime could be due to two possible reasons. According to the previous report,[40,41] TiO_2 is known to contain many oxygen vacancies (or Ti^{3+} sites), particularly on the surface, corresponding to the trap states. In the low temperature processed TiO_2 compact layer used in this work, the mixing nature of the crystal TiO_2 and amorphous TiO_X gives an even higher trap density. Lewis base groups like —CN and —SCN[40] have been proven to occupy the oxygen vacancies (or Ti^{3+} sites), and thus to pacify oxygen vacancies.[40] In such a scenario, the adsorption of electron-withdrawing groups, considering both —CN and carbon ball, on oxygen vacancies (Ti^{3+}) will dramatically reduce the charge trapping effect. Consequently, the passivation of the TiO_2 surface by PCBB-2CN-2C8 could be responsible for the long carrier lifetime. Similar explanations have been invoked to describe reductions in carrier recombination due to changes in the electrode chemistry in perovskite[42] and organic solar cells.[43]

The electronic trap states are able to delocalize charge carriers and to induce high capacitance at the interface, which can be readily detected using impedance spectroscopy. To further confirm the hypothesis that PCBB-2CN-2C8 pacifies the trap states on the TiO_2 surface, we performed impedance measurements on the perovskite solar cells of ITO/TiO_2/with or without PCBB-2CN-2C8/$CH_3NH_3PbI_3$/spiro-OMeTAD/Au at 1 kHz frequency. We extracted capacitance–voltage characteristics as shown in Figure 7. At this frequency, obvious

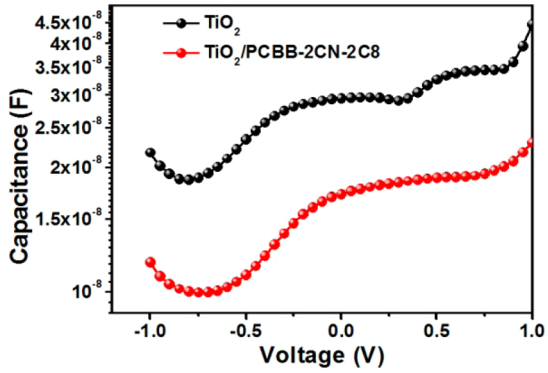

Figure 7. Capacitance–voltage characteristics of the optimized perovskite solar cells employing the TiO_2 and TiO_2/PCBB-2CN-2C8 as ETLs.

variation of capacitance occurs with increasing bias voltage, which is indicative of charge accumulation at the compact layer and can represent its capacitance.[21] With PCBB-2CN-2C8 modification, the capacitances of devices are unambiguously reduced, confirming the passivation effect of PCBB-2CN-2C8 as discussed above.[40,41] It leads us to the conclusion that the higher current extraction ability and longer lifetime in a TiO_2/PCBB-2CN-2C8-based device is predominated by the reduced TiO_2 trap state.

As mentioned earlier, UV irradiation causes fast release of O_2 on the TiO_2 surface, and induces a large amount of deep trap states. According to the report by Snaith's group, it is responsible for the fast degradation of the perovskite solar cells. Therefore, we looked into the stability issue to confirm the passivation effect. The devices using TiO_2 as an ETL with and without PCBB-2CN-2C8 were investigated for comparison. Stored on a windowsill under ambient air without encapsulation allows 6 h exposure to natural sunlight per day at a humidity of 45–50%. The normalized PCEs and J_{sc} vs time from 10 devices for each structure are summarized in Figure 8. TiO_2 based control devices showed 5.6% of the initial PCE after 120 h exposure, accompanying the significantly decreased J_{sc} to 30% of their initial values. In the meantime, the device based on PCBB-2CN-2C8-coated TiO_2 showed a significant improvement in stability under prolonged illumination, retaining more than 60% and 90% of their initial efficiency and photocurrent, respectively, after 500 h exposure.[44] In terms of chemistry, the origin of this effect is possibly caused by the TiO_2 photocatalyst degredation of the perovskite film,[19,45] and electrically, the creation of a large density of deep trap sites on ultraviolet excitation on TiO_2 surface.[18] The main point of the

DOI: 10.1021/jacs.5b10614
J. Am. Chem. Soc. 2015, 137, 15540–15547

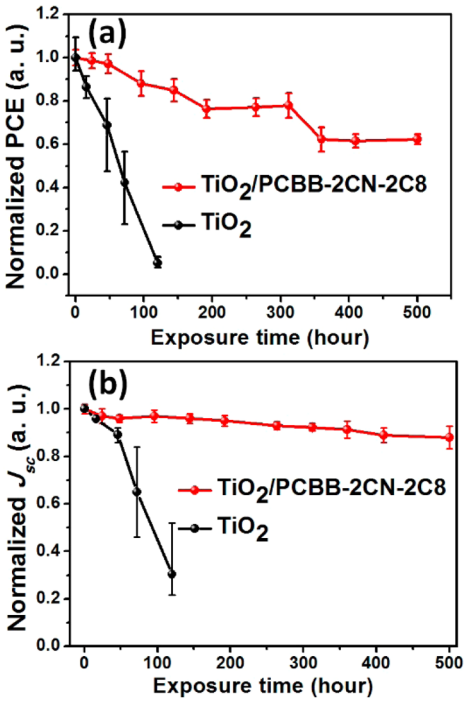

Figure 8. (a) The efficiency and (b) short current density evolution of the unencapsulated devices stored on a windowsill in ambient air with the humidity of 45−50%.

stability test is to further confirm passivation of surface trap states of TiO_2.

In summary, we have synthesized a triblock functionalized fullerene derivative PCBB-2CN-2C8 for ETL interface engineering on low temperature-processed TiO_2 in the planar n-i-p perovskite solar cells. The molecule design theme allows us simultaneously address several major challenges, including processing compatibility for multilayer coating, interface recombination loss, work function tuning of electrodes, the notorious hysteresis and interface induced device degradation, via simple and fast solution spin-coating process. We proposed that the passivation of the TiO_2 surface by PCBB-2CN-2C8 on it is an effective approach to enhance the photovoltaic performance, as supported by both materials characterization and device analysis. Interestingly, the encouraging stability data imply that surface passivation is a promising strategy to avoid the rapid degradation caused by the UV sensitive TiO_2 surface.

EXPERIMENTAL SECTION

Materials Synthesis. *Dimethyl 5-Hydroxyisophthalate (1).* To the solution of 5-hydroxyisophthalic acid (10 g, 0.054 mol) in CH_3OH (200 mL), 10 drops H_2SO_4 was added, and the mixture was refluxed for 5 h. Then the reaction mixture was poured into saturated sodium bicarbonate solution and stirred for 0.5 h. Then the solution was filtered to give dimethyl 5-hydroxyisophthalatein 84.1% yield as a white solid. ^{1}H NMR (400 MHz, $CDCl_3$): δ(ppm) 8.26 (s, J = 1.4 Hz, 1H), 7.74 (s, J = 1.4 Hz, 2H), 5.83 (s, 1H), 3.95 (s, 6H).

(5-Hydroxy-1,3-phenylene)dimethanol (2). $LiAlH_4$ (1.448 g, 38.095 mmol) was added in the THF (100 mL) solution of dimethyl 5-hydroxyisophthalate (2 g, 9.524 mmol) under the protection of an Ar in ice-bath and stirred at room temperature for 24 h. Then the reaction mixture was quenched by HCl solution. The product was extracted with ethyl acetate three times. The combined organic layers were dried over anhydrous Na_2SO_4. After filtration and evaporation, the residue was purified by silica gel chromatography with petroleum ether: ethyl ester (1/5 v/v). The yield is 66.5% as a colorless oil.^{1}H NMR (400 MHz, DMSO): δ(ppm) 9.21 (s, 1H), 6.66 (s, 1H), 6.59 (s, 2H), 5.08 (t, J = 5.8 Hz, 2H), 4.39 (d, J = 5.8 Hz, 4H).

5-Hydroxyisophthalaldehyde (3). To the solution of (5-hydroxy-1,3-phenylene)dimethanol (1 g, 6.494 mmol) in THF (20 mL) and CH_2Cl_2 (30 mL) was added SiO_2 (4.169 g, 69.481 mmol) and PCC (4.199 g, 19.481 mmol). The reaction mixture was stirred at room temperature for 12 h. Then the product was purified by silica gel chromatography with petroleum ether/ethyl ester (5/1, v/v). The yield is 50.5% as a white solid. ^{1}H NMR (400 MHz, DMSO): δ(ppm)10.53 (s, 1H), 10.03 (s, 2H), 7.91 (s, 1H), 7.56 (s, 2H).

Dioctyl-3,3′-(5-hydroxy-1,3-phenylene)-bis(2-cyanoacrylate) (4). 5-Hydroxyisophthalaldehyde (1 g, 6.667 mmol), octyl 2-cyanoacetate (2.629 g,13.333 mmol) was added to ethanol (5 mL) and water (2 mL), and then several drops of $(NH_4)_2HPO_3$ were added. The reaction mixture was stirred at room temperature for 12 h. After reaction, the solution was filtrated, and the filter residue was purified by silica gel chromatography with petroleum ether: ethyl ester (3/1 v/v) to give in 89.4% yield as a kelly solid. ^{1}H NMR (400 MHz, $CDCl_3$): δ(ppm) 8.21 (s, 2H), 7.79 (s, 3H), 6.32 (s, 1H), 4.33 (t, J = 6.7 Hz, 4H), 1.82−1.72 (m, 4H), 1.42 (m, 4H), 1.30 (m, J = 10.8 Hz, 16H), 0.88 (t, J = 7.0 Hz, 6H).

[6,6]-Phenyl-C_{61}-butyric Acid-dioctyl-3,3′-(5-hydroxy-1,3-phenylene)-bis(2-cyanoacrylate)ester (PCBB-2CN-2C8). To a flask, PCBA (0.1 g, 0.112 mmol), dioctyl 3,3′-(5-hydroxy-1,3-phenylene)-bis(2-cyanoacrylate)(0.057 g, 0.112 mmol), DMAP(0.014 g, 0.112 mmol), PTSA(0.021 g, 0.112 mmol) was added. Then DIPC(0.020 g, 0.157 mmol) was washed into it by dichlorobenzene(30 mL), stirred at room temperature for 12 h with the protection of Ar. Then the solution was filtered, and the filtrate was purified by silica gel chromatography with petroleum ether/toluene(1/3 v/v). The crude product was suspended in methanol to give PCBB-2CN-2C8 in 66.5% yield as a brown solid. ^{1}H NMR (400 MHz, $CDCl_3$): δ(ppm) 8.23 (s, 2H), 8.17 (s, 1H), 7.96 (d, J = 8.5 Hz, 4H), 7.57 (t, J = 7.6 Hz, 2H), 7.50 (t, J = 7.3 Hz, 1H), 4.34 (t, J = 6.7 Hz, 4H), 3.02 (t, 2H), 2.85 (t, J = 7.2 Hz, 2H), 2.34 (m, 2H), 1.82−1.70 (m, 4H), 1.42 (m, 4H), 1.29 (m, J = 11.8 Hz, 16H), 0.88 (t, J = 6.9 Hz, 6H)^{13}C NMR (400 MHz, $CDCl_3$) δ 170.80, 161.54, 151.99, 151.43, 148.66, 147.65, 145.14, 145.02, 144.75, 144.61, 144.46, 144.39, 143.71, 143.00, 142.95, 142.87, 142.14, 142.08, 140.99, 140.72, 137.96, 137.55, 136.52, 133.65, 132.06, 130.69, 128.54, 128.36, 126.83, 114.53, 106.19, 79.71, 67.29, 51.58, 33.98, 33.49, 31.74, 29.13, 28.43, 25.73, 22.63, 22.14, 14.12. MALDI-TOF MS: Calcd. for$C_{113}H_{50}N_2O_6$: 1386.37; Found: 1386.48.

Device Fabrication. Methylammonium iodide (CH_3NH_3I, MAI) and methylammonium chloride (CH_3NH_3Cl, MACl) were synthesized using the method described elsewhere.[6] The TiO_2 nanocrystals were obtained from a nonhydrolytic sol−gel approach.[6] ITO glass substrates were sequentially washed with isopropanol, acetone, distilled water, and ethanol. The TiO_2 ETL was subsequently spin-coated on ITO substrates with a TiAcac-stabilized TiO_2 solution at 3000 rpm and annealed at 150 °C for 30 min in air. The second TiO_2 ETL was fabricated according to the above process. Then PCBB-2CN-2C8 (dissolved in CB, 5 mg/mL) was spin-coated on TiO_2 at 3000 rpm for 30 s, and dried in vacuum chamber for 1 h. A 70 °C PbI_2 solution (dissolved in DMF, 460 mg/mL) was spin-coated on top of ITO/TiO_2/PCBB-2CN-2C8 substrate at 3000 rpm for 30 s, and kept on a hot plate at 75 °C for 10 min. Then a mixture of MAI/MACl (50 mg/mL:5 mg/mL, dissolved in 2-propanol) was spin-coated on top of the dried PbI_2 layer at room temperature at 4000 rpm for 40 s in a nitrogen-filled glovebox. All of the films were annealed in the air at 135 °C for 20 min. A hole transport layer solution was coated on the perovskite film at 3000 r.p.m. for 30 s, where a spiro-OMeTAD/chlorobenzene (90 mg/mL) solution was employed with addition of 45 mL Li-TFSI/acetonitrile (170 mg/mL) and 10 mL tBP. Finally, the counter electrode was deposited by thermal evaporation of gold under a pressure of 5×10^{-5} Torr. The active area was 0.108 cm^2. The details for characterization are described in the SI.

DOI: 10.1021/jacs.5b10614
J. Am. Chem. Soc. 2015, 137, 15540−15547

■ ASSOCIATED CONTENT

Supporting Information

The Supporting Information is available free of charge on the ACS Publications website at DOI: 10.1021/jacs.5b10614.

Detailed material and device characterization. Additional figures showing TGA thermograms; DSC analysis; $J-V$ characteristics; ^{1}H NMR spectrum; ^{13}C NMR spectrum; MALDI-TOF mass spectrum; the images of water and DMF droplets contact angles; the AFM height and SKPM images; grain size distribution of the perovskite film; transmittance spectra; EQE spectrum; and additional references (PDF)

■ AUTHOR INFORMATION

Corresponding Authors

*ywli@suda.edu.cn
*zrhong@ucla.edu
*liyongfang@suda.edu.cn
*yangy@ucla.edu

Notes

The authors declare no competing financial interest.

■ ACKNOWLEDGMENTS

Y.L. acknowledged for financial support from Jiangsu Government Scholarship for Overseas Studies. Vishal Bharti for SCLC test. This work was partially supported by the National Natural Science Foundation of China (Grant No. 21204057). Priority Academic Program Development of Jiangsu Higher Education Institutions. National Science Foundation (Grant Number ECCS-1509955, Program Director Dr. Nadia El-Masry), Air Force Office of Scientific Research (Grant Number FA9550-15-1-0333, Program Director Dr. Charles Lee).

■ REFERENCES

(1) Kojima, A.; Teshima, K.; Shirai, Y.; Miyasaka, T. *J. Am. Chem. Soc.* **2009**, *131*, 6050.
(2) Lee, M. M.; Teuscher, J.; Miyasaka, T.; Murakami, T. N.; Snaith, H. J. *Science* **2012**, *338*, 643.
(3) Kim, H.-S.; Lee, C.-R.; Im, J.-H.; Lee, K.-B.; Moehl, T.; Marchioro, A.; Moon, S.-J.; Humphry-Baker, R.; Yum, J.-H.; Moser, J. E.; Grätzel, M.; Park, N.-G. *Sci. Rep.* **2012**, *2*, 591.
(4) Liu, M.; Johnston, M. B.; Snaith, H. J. *Nature* **2013**, *501*, 395.
(5) Lee, J.-W.; Seol, D.-J.; Cho, A.-N.; Park, N.-G. *Adv. Mater.* **2014**, *26*, 4991.
(6) Zhou, H.; Chen, Q.; Li, G.; Luo, S.; Song, T.-b.; Duan, H.-S.; Hong, Z.; You, J.; Liu, Y.; Yang, Y. *Science* **2014**, *345*, 542.
(7) Yang, W. S.; Noh, J. H.; Jeon, N. J.; Kim, Y. C.; Ryu, S.; Seo, J.; Seok, S. I. *Science* **2015**, *348*, 1234.
(8) Shi, J.; Xu, X.; Li, D.; Meng, Q. *Small* **2015**, *11*, 2472.
(9) Abrusci, A.; Stranks, S. D.; Docampo, P.; Yip, H.-L.; Jen, A. K. Y.; Snaith, H. J. *Nano Lett.* **2013**, *13*, 3124.
(10) Kuang, C.; Tang, G.; Jiu, T.; Yang, H.; Liu, H.; Li, B.; Luo, W.; Li, X.; Zhang, W.; Lu, F.; Fang, J.; Li, Y. *Nano Lett.* **2015**, *15*, 2756.
(11) Azimi, H.; Ameri, T.; Zhang, H.; Hou, Y.; Quiroz, C. O. R.; Min, J.; Hu, M.; Zhang, Z.-G.; Przybilla, T.; Matt, G. J.; Spiecker, E.; Li, Y.; Brabec, C. J. *Adv. Energy Mater.* **2015**, *5*, 1401692.
(12) Liu, X.; Yu, H.; Yan, L.; Dong, Q.; Wan, Q.; Zhou, Y.; Song, B.; Li, Y. *ACS Appl. Mater. Interfaces* **2015**, *7*, 6230.
(13) Docampo, P.; Ball, J. M.; Darwich, M.; Eperon, G. E.; Snaith, H. J. *Nat. Commun.* **2013**, *4*, 2761.
(14) Wang, Q.; Shao, Y.; Dong, Q.; Xiao, Z.; Yuan, Y.; Huang, J. *Energy Environ. Sci.* **2014**, *7*, 2359.
(15) Wojciechowski, K.; Saliba, M.; Leijtens, T.; Abate, A.; Snaith, H. J. *Energy Environ. Sci.* **2014**, *7*, 1142.
(16) Kim, H.-S.; Mora-Sero, I.; Gonzalez-Pedro, V.; Fabregat-Santiago, F.; Juarez-Perez, E. J.; Park, N.-G.; Bisquert, J. *Nat. Commun.* **2013**, *4*, 2242.
(17) Snaith, H. J.; Abate, A.; Ball, J. M.; Eperon, G. E.; Leijtens, T.; Noel, N. K.; Stranks, S. D.; Wang, J. T.-W.; Wojciechowski, K.; Zhang, W. *J. Phys. Chem. Lett.* **2014**, *5*, 1511.
(18) Leijtens, T.; Eperon, G. E.; Pathak, S.; Abate, A.; Lee, M. M.; Snaith, H. J. *Nat. Commun.* **2013**, *4*, 2885.
(19) Ito, S.; Tanaka, S.; Manabe, K.; Nishino, H. *J. Phys. Chem. C* **2014**, *118*, 16995.
(20) Tao, C.; Neutzner, S.; Colella, L.; Marras, S.; Srimath Kandada, A. R.; Gandini, M.; Bastiani, M. D.; Pace, G.; Manna, L.; Caironi, M.; Bertarelli, C.; Petrozza, A. *Energy Environ. Sci.* **2015**, *8*, 2365.
(21) Wojciechowski, K.; Stranks, S. D.; Abate, A.; Sadoughi, G.; Sadhanala, A.; Kopidakis, N.; Rumbles, G.; Li, C.-Z.; Friend, R. H.; Jen, A. K. Y.; Snaith, H. J. *ACS Nano* **2014**, *8*, 12701.
(22) Zhang, Y.; Yip, H.-L.; Acton, O.; Hau, S. K.; Huang, F.; Jen, A. K. Y. *Chem. Mater.* **2009**, *21*, 2598.
(23) Leijtens, T.; Lim, J.; Teuscher, J.; Park, T.; Snaith, H. J. *Adv. Mater.* **2013**, *25*, 3227.
(24) Bi, C.; Wang, Q.; Shao, Y.; Yuan, Y.; Xiao, Z.; Huang, J. *Nat. Commun.* **2015**, *6*, 7747.
(25) Liu, C.; Wang, K.; Du, P.; Meng, T.; Yu, X.; Cheng, S. Z. D.; Gong, X. *ACS Appl. Mater. Interfaces* **2015**, *7*, 1153.
(26) Chen, Q.; Zhou, H.; Fang, Y.; Stieg, A. Z.; Song, T.-B.; Wang, H.-H.; Xu, X.; Liu, Y.; Lu, S.; You, J.; Sun, P.; McKay, J.; Goorsky, M. S.; Yang, Y. *Nat. Commun.* **2015**, *6*, 7269.
(27) Shimizu, H.; Cojal González, J. D.; Hasegawa, M.; Nishinaga, T.; Haque, T.; Takase, M.; Otani, H.; Rabe, J. P.; Iyoda, M. *J. Am. Chem. Soc.* **2015**, *137*, 3877.
(28) Zhou, H.; Zhang, Y.; Mai, C.-K.; Collins, S. D.; Bazan, G. C.; Nguyen, T.-Q.; Heeger, A. J. *Adv. Mater.* **2015**, *27*, 1767.
(29) Docampo, P.; Hanusch, F. C.; Stranks, S. D.; Döblinger, M.; Feckl, J. M.; Ehrensperger, M.; Minar, N. K.; Johnston, M. B.; Snaith, H. J.; Bein, T. *Adv. Energy Mater.* **2014**, *4*, 1400355.
(30) Bi, C.; Shao, Y.; Yuan, Y.; Xiao, Z.; Wang, C.; Gao, Y.; Huang, J. *J. Mater. Chem. A* **2014**, *2*, 18508.
(31) Liu, D.; Kelly, T. L. *Nat. Photonics* **2013**, *8*, 133.
(32) Burschka, J.; Pellet, N.; Moon, S.-J.; Humphry-Baker, R.; Gao, P.; Nazeeruddin, M. K.; Gratzel, M. *Nature* **2013**, *499*, 316.
(33) Malinkiewicz, O.; Yella, A.; Lee, Y. H.; Espallargas, G. M.; Graetzel, M.; Nazeeruddin, M. K.; Bolink, H. J. *Nat. Photonics* **2014**, *8*, 128.
(34) Kim, H.-S.; Park, N.-G. *J. Phys. Chem. Lett.* **2014**, *5*, 2927.
(35) Yu, J. C.; Kim, D. B.; Baek, G.; Lee, B. R.; Jung, E. D.; Lee, S.; Chu, J. H.; Lee, D.-K.; Choi, K. J.; Cho, S.; Song, M. H. *Adv. Mater.* **2015**, *27*, 3492.
(36) Liang, P.-W.; Liao, C.-Y.; Chueh, C.-C.; Zuo, F.; Williams, S. T.; Xin, X.-K.; Lin, J.; Jen, A. K. Y. *Adv. Mater.* **2014**, *26*, 3748.
(37) Zuo, L.; Gu, Z.; Ye, T.; Fu, W.; Wu, G.; Li, H.; Chen, H. *J. Am. Chem. Soc.* **2015**, *137*, 2674.
(38) Abate, A.; Saliba, M.; Hollman, D. J.; Stranks, S. D.; Wojciechowski, K.; Avolio, R.; Grancini, G.; Petrozza, A.; Snaith, H. J. *Nano Lett.* **2014**, *14*, 3247.
(39) Credgington, D.; Durrant, J. R. *J. Phys. Chem. Lett.* **2012**, *3*, 1465.
(40) Schwanitz, K.; Weiler, U.; Hunger, R.; Mayer, T.; Jaegermann, W. *J. Phys. Chem. C* **2007**, *111*, 849.
(41) Schwanitz, K.; Mankel, E.; Hunger, R.; Mayer, T.; Jaegermann, W. *Chimia* **2007**, *61*, 796.
(42) Nagaoka, H.; Ma, F.; deQuilettes, D. W.; Vorpahl, S. M.; Glaz, M. S.; Colbert, A. E.; Ziffer, M. E.; Ginger, D. S. *J. Phys. Chem. Lett.* **2015**, *6*, 669.
(43) Knesting, K. M.; Ju, H.; Schlenker, C. W.; Giordano, A. J.; Garcia, A.; Smith, O. N. L.; Olson, D. C.; Marder, S. R.; Ginger, D. S. *J. Phys. Chem. Lett.* **2013**, *4*, 4038.
(44) Stranks, S. D.; Snaith, H. J. *Nat. Nanotechnol.* **2015**, *10*, 391.
(45) Fujishima, A.; Rao, T. N.; Tryk, D. A. *J. Photochem. Photobiol., C* **2000**, *1*, 1.

DOI: 10.1021/jacs.5b10614
J. Am. Chem. Soc. 2015, 137, 15540−15547